Interdiffusion of Polymers at Short Times

ARTICLE *in* MACROMOLECULES · NOVEMBER 1994

Impact Factor: 5.8 · DOI: 10.1021/ma00101a039

3 AUTHORS, INCLUDING:

Alamgir Karim
University of Akron
307 PUBLICATIONS **6,938** CITATIONS

SEE PROFILE

Interdiffusion of Polymers at Short Times

A. Karim[†] and G. P. Felcher

Argonne National Laboratory, Argonne, Illinois 60439

T. P. Russell[*]

IBM Research Division, Almaden Research Center, 650 Harry Road, San Jose, California 95120

Received May 20, 1994; Revised Manuscript Received August 23, 1994[⊗]

ABSTRACT: The short-time interdiffusion between bilayers of protonated and deuterated polystyrene was measured using neutron reflectivity. The moments of the segment density profiles were used as a model-independent means of characterizing the interdiffusion. It is shown that for diffusion times between the Rouse relaxation time and the reptation time of a single chain, the concentration profile at the polymer/polymer interface can be described by a sharp gradient at the interface with a relatively long range decay away from it. With increasing molecular weight, the decay length increased substantially as expected for reptating chains. Furthermore, the effective diffusion coefficient is shown to decrease for all times less than the estimated reptation time and reduce to the bulk value at longer times. Critical slowing down effects of isotropic origin at the interface are shown to be of no consequences in these studies.

Introduction

The interdiffusion in melts of high molecular weight homopolymers has received considerable experimental and theoretical attention. The connectivity of the monomers and the entanglements of these long-chain molecules place severe restrictions on the chain dynamics. Most studies have focused on diffusion lengths much larger than the size of the diffusing molecule.[1] Notably, some earlier studies include infrared microdensitometry by Klein and co-workers,[2] forward recoil spectrometry by Kramer and co-workers,[3,4] and, more recently, secondary ion mass spectrometry by Wood et al.[5] These studies have shown that the reptation model of de Gennes[6,7] and Doi and Edwards,[8] with its extension by Graessley,[9] can explain experimental observations over a large range of molecular weights, temperatures, and compositions. In particular, these studies confirmed that the diffusion coefficient $D \sim D_0/N^2$, where D_0 depends on the chain architecture and N is the number of segments in the polymer. While these studies support, they do not prove reptation unequivocally. Critical differences between various theories are seen only at short times, i.e., over diffusion distances less than R_g, the radius of gyration of the molecule. Experiments to examine such short length scales, with the exception of the computer simulations of Kremer et al.[10] and the neutron spin echo studies of Richter and co-workers,[11] have been lacking for want of a technique with sufficient depth resolution. Neutron reflectivity with a depth resolution of ~10 Å has made it possible to test some of these fundamental predictions.[12-17] More recently, dynamic secondary ion mass spectroscopy, coupled with a selective chain labeling, has also provided some strong evidence supporting reptation arguments.[18]

The reptation model proposed by de Gennes is a simple and visual model for the dynamics of entangled molecules in a network of fixed obstacles. Here, the polymer molecule slides or "reptates" through a "tube" whose contour is defined by the locus of entanglements with neighboring molecules. The motion of the molecule transverse to the contour of the tube is severely restricted. While this description seems simple, it has been able to predict correctly the results of diffusion over large distances, i.e., for $\langle r^2 \rangle^{1/2} \gg R_g$ where $\langle r^2 \rangle$ is the mean square displacement of the molecules.

The restriction on the transverse motion of chains was relaxed to allow for Rouse type motions within the tube.[19] Within the Doi–Edwards framework over distances less than an entanglement length, Brownian motion of coupled oscillators (Rouse dynamics) is applicable whereas over larger distances the sliding motion (reptation dynamics) of the chain along its own contour occurs. Thus, the diffusion at times less than the reptation time is predicted to be nonclassical. Three characteristic times emerge from such a description of the dynamics of the molecule.[8] First, there is the entanglement Rouse time, τ_e, which is defined as the time at which the displacement of chain segments of entanglement molecular weight becomes comparable to the tube diameter. Second, there is the Rouse relaxation time, τ_R, which is the time when the motion of the single segments becomes coordinated over the entire length of the chain. Finally there is the reptation or tube disengagement time, τ_d, which is the time required for complete disengagement of the chain from its initial "tube". In these time regimes, the predicted mean square displacement of monomers, $\langle x^2 \rangle$, does not evolve with time, t, as in a conventional diffusion process but rather as t^α, where $\alpha < 1$, becoming 1 only beyond the reptation time. At times $t < \tau_e$, the motion of monomers is essentially the same as in a Rouse model in free space and $\alpha = 1/2$. At slightly longer times between τ_e and τ_R, the motion is partly Rouse-like and partly reptative and $\alpha = 1/4$. At still longer times, reptation is the dominant motion and $\alpha = 1/2$. For $t > \tau_d$ the molecule diffuses effectively as an entity and conventional diffusion behavior ($\alpha = 1$) should be recovered.

A distinctive signature of reptative motion is predicted for the interdiffusion profile at the interface between two polymer melts brought in contact, since only the molecules whose chain ends are at the interface can cross the interface. A discontinuity of the concentration profile at the interface should persist up to τ_d whereupon an error function profile is recovered. The time evolution of the concentration profile across the interface has been described by de Gennes,[20,21] Tirrell and co-workers,[22,23] and Wool et al.[24-26] In reality, the discontinuity of the concentration profile is expected to be almost instantly smeared out by segmental (Rouse) motion over a distance

[†] Present address: Polymers Division, NIST, Gaithersburg, MD.
[⊗] Abstract published in *Advance ACS Abstracts,* October 1, 1994.

0024-9297/94/2227-6973$04.50/0

Table 1. Parameters of the Polymers within the Framework of the Reptation Theory

M_w	2.33×10^5	1.03×10^6
R_g (Å)	130	264
D (cm^2/s)	5.45×10^{-18} [a]	6.08×10^{-16} [b]
τ_e (s)	5.6[a]	2.0×10^{-3}
τ_R (s)	672.0[a]	5.4[b]
τ_D (s)	6.24×10^4 [a]	2340[b]

[a] At 120 °C. [b] At 155 °C.

corresponding to the distance between entanglement points. It is easier to deconvolve this rapid and almost constant interfacial broadening from the long-range decaying profile due to reptation in high molecular weight polymers where the two widths are better separated.

In this study, the time evolution of the concentration profile across an interface between polystyrene and perdeuterated polystyrene has been investigated by neutron reflectivity. These studies have focused on the concentration profile at times less than τ_d and, hence, over distances less than R_g. The results are compared with the different aspects of the phenomenology expected on the basis of the reptation model. As shown, most of the observations are in accord with this model.

Experimental Section

Measurements were done on polystyrene homopolymers having molecular weights of $\sim 2 \times 10^5$ and $\sim 1 \times 10^6$. Both normal polystyrene (h-PS) and perdeuterated polystyrene (d-PS) with narrow molecular weight distributions (typically $M_w/M_n < 1.05$) were purchased from Polymer Laboratories. These were characterized by size exclusion chromatography and used without further purification. Specimens were prepared by dissolving the h-PS or d-PS in toluene to produce a 3% (w/v) solution. A polished 5 cm diameter silicon substrate (5 mm in thickness) was spin coated with this solution. This left a film of the h-PS or d-PS on the surface which was dried and annealed under vacuum for 48 h at 160 °C. The thickness of the film depended upon the molecular weight, concentration, and spinning speed of the h-PS or d-PS. In general, films of at least 2×10^3 Å were used. A second film was prepared on a 7.5 × 12.5 cm microscope slide in a similar manner. By variation of the concentration, film thicknesses from 600 to 10^3 Å were obtained. Without annealing or extensively drying the film, the sides of the microscope slide were scored with a razor blade and the film was floated off onto a pool of deionized water. The film was then retrieved, with the polymer-coated silicon substrate forming a bilayered specimen. This bilayer was then placed under vacuum at room temperature for ~12 h to remove residual solvent and water trapped between the layers. As discussed in detail in a previous study, not all the water is removed from the interface via this route.[27] However, it was shown that this did not perturb the interdiffusion of the polymers at the interface. It should be mentioned that creasing or cracking of the transferred layer occurred occasionally but such defects comprised only a small fraction of the entire surface and can be ignored.

Interdiffusion was accomplished by placing the bilayer specimen in a preheated oven specifically designed for these studies. Clearance between the floor and ceiling of the oven and the silicon substrate was small, thereby maximizing the transfer of heat from the specimen. This was augmented by use of a helium atmosphere which also served to retard degradation of the polymer layers. Approximately 30 s was required for the specimen to reach the desired temperature for the interdiffusion experiments. Depending upon the time scale of interest and the molecular weights of the polymers, the temperature was adjusted such that the heating time was small in comparison to the interdiffusion time. Annealing temperatures and times were chosen to maximize the observation range. To this end the typical parameters pertaining to the reptation model were used as obtained from the literature and are summarized in Table 1. After the desired interdiffusion time, the specimens were quenched to room temperature by placing the substrate on a cool metal block. The time required to cool the specimen to below the glass transition temperature, $T_g \sim 100$ °C, was less than 10 s and was, hence, of no consequence. All reflectivity exeriments were performed at room temperature.

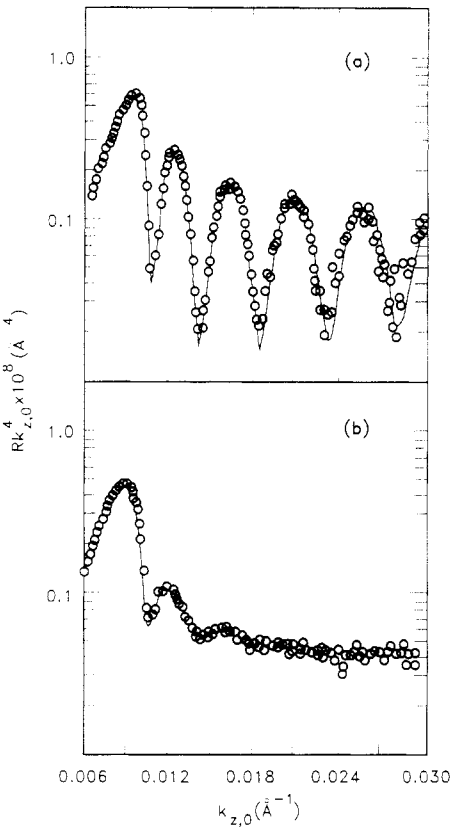

Figure 1. Rk^4 as a function of k for a bilayered sample of d-PS (M_w = 233 000) on top of h-PS (M_w = 203 000) before heating (a) and after heating for 22 min (b) at 135 °C. The circles are the experimental data whereas the solid lines were calculated using a bilayered model with a symmetric interface between the upper and lower layers as described in the text.

Neutron reflectivity measurements were performed using the neutron reflectometer POSY-II at the Intense Pulsed Neutron Source at the Argonne National Laboratory. Details of the instrument can be found elsewhere.[28,29] Briefly, a collimated beam of neutrons with a distribution of wavelengths from 2 to 15 Å impinges on the specimen mounted vertically on a goniometer that allows the specimen to be rotated to the desired angle of incidence with the goniometer. The reflected and refracted neutrons pass through a helium-filled flight path to minimize air scattering and then onto a gas-filled position-sensitive proportional counter. The refracted neutrons are intercepted by a beam stop prior to the detector. Via standard time of flight procedures, the reflectivity as a function of the neutron momentum normal to the film surface, $k_{z,0}$, is obtained, where $k_{z,0} = (2\pi/\lambda) \sin \theta$. Here, λ is the wavelength, θ is the incidence angle, and the subscripts denote in the z-direction, i.e., normal to the film surface, and in vacuum, 0. The instrumental resolution at different incidence angles, $\Delta k_{z,0}/k_{z,0}$, was determined by independent reflectivity measurements on standards and was incorporated into the calculated reflectivity profiles. Two angles of incidence, typically 0.3 and 1.0°, were required to cover the desired momentum range.

A typical set of neutron reflectivity profiles are shown in Figure 1a,b. These data correspond to a bilayer comprised of a top layer of d-PS (M_w = 233 000) on a thick lower layer of h-PS (M_w = 203 000) prior to heating (a) and after heating to 135 °C for 22 min (b). The data are plotted as the reflectivity, R, times $k_{z,0}^4$ as a function of $k_{z,0}$ since, for a system containing a sharp interface, the mean value of $Rk_{z,0}^4$, at large $k_{z,0}$, approaches a constant value proportional to the sum of the square of the reflectances at the sharp interfaces. The data in Figure 1a for the unheated specimen exhibit a clear series of sharp oscillations where at high $k_{z,0}$ the

Table 2. Lower Molecular Weight Polymers: Annealing Time and Diffusion Characteristics

bilayer	layer thickness (Å)	annealing temp (°C)	annealing time (min)	effective annealing time at 120 °C (min)	$\langle z^2\rangle^{1/2}$	$\langle z^4\rangle^{1/4}$
(1) D203K/H233K	600/2886	130	5	68	42	55.3
			49	669	106	139.5
			139	1899	155	204.0
(2) D203K/H233K	600/2000	105.5	30	0.126	21	27.6
		135	22	881	88	115.8
			53	2122	135	177.7
(3) D203K/H233K	1080/982	120	10	10	28	36.9
		130.7	22.4	369	64	84.2
		135	12.5	869	106	139.5
(4) H233K/D550 K	980/3500	125	10	40	39	51.3
			30	121	49	64.5
			70	282	53	70.0
			150	605	71	93.4
			310	1250	88	115.8
(5) H233K/D550K	990/2300	116.3	10	3	28	36.9
			110	34	46	60.5
			180	56	49	64.5
			2340	728	102	134.2
			9840	3061	141	185.6
(6) H475K/D205K	675/1775	116.3	15	4.7	38	50
			30	9.3	42	55.3
			9405	2925	112	147.4
(7) H475K/D205K	675/1850	105.5	2	0.0084	21	27.6
			62	0.26	28	36.9
			1322	5.57	42	55.3

difference in the values of $k_{z,0}$ of successive minima ($\Delta k_{z,0}$) yields directly the thickness of the top d-PS layer from $d = \pi/(\Delta k_{z,0})$. In this case, the thickness of the d-PS layer, 600 Å, matches the value of 590 Å measured by optical ellipsometry on a d-PS film prepared in an identical manner. The thickness of the lower h-PS layer is 2000 Å as measured ellipsometrically. Neutron reflectivity measurements are insensitive to the thickness of the lower h-PS layer for two reasons. Oscillations in the reflectivity profile arising from a film of this thickness occur at a frequency Δk almost as high as the resolution of the instrument. Secondly, the reflectances at the air/d-PS and d-PS/h-PS interfaces are much larger than those at the h-PS/Si interface, and, consequently, the amplitudes of the oscillations in the reflectivity arising from the h-PS layer are much smaller than those from the d-PS layer. The solid line in the figure was calculated using a bilayer model of d-PS with a thickness of 600 Å having a scattering length density, (b/V), of 6.4×10^{-6} Å^{-2} on top of a 2000 Å layer of h-PS with $(b/V) = 1.43 \times 10^{-6}$ Å^{-2}. A symmetric interface described by an error function with a width of 10 Å was also used.

Heating this bilayer to 135 °C for 22 min causes an interdiffusion of the h-PS and d-PS layers and, therefore, results in a broadening of the interface between the two layers. The effect on the reflectivity profile is dramatic. While the oscillations characteristic of the d-PS layer are still evident, they are markedly damped. In addition, the mean value of $Rk_{z,0}^4$ at high $k_{z,0}$ approaches a lower asymptotic value than the data for the unheated specimen. These are direct consequences of the broadening of the interface between the d-PS and h-PS layers. The solid line in Figure 1b was calculated using a bilayer model with the same thickness and (b/V) values as in the unheated specimen but with an increases interface width of 125 Å between the h-PS and d-PS layers.

To view the affect of interface broadening analytically, consider the situation where a deuterated layer of thickness d is in contact with an infinitely thick protonated layer. The reflectivity then assumes the simple form

$$R = \left| \frac{r_{VD} + r_{DH} \exp(2ik_D d)}{1 + r_{VD} r_{DH} \exp(2ik_D d)} \right|^2 \tag{1}$$

where r_{VD} and r_{DH} are the reflectances at the vacuum/deuterated polymer and the deuterated/protonated polymer interfaces, respectively. The reflectances are defined as

$$r_{ij} = \frac{k_i - k_j}{k_i + k_j} \tag{2}$$

where $k_i = [k_0^2 - 4\pi(b/v)_i]^{1/2}$ is the neutron momentum in medium i with a scattering length density $(b/V)_i$.

Suppose now that a conventional or Fickian diffusion occurs. This would produce a variation in the concentration of the deuterated component, C_D, across the interface given by

$$C_D = \frac{1}{2} \operatorname{erfc}[(z - z_D)/(2\langle z^2\rangle)^{1/2}] \tag{3}$$

where erfc is the error function complement and $\langle z^2\rangle$ is the mean square thickness of the interface. In this case, the reflectance of the specimen is given by

$$r_{DH} = \frac{k_D - k_H}{k_D + k_H} \exp(-k_D k_H / \langle z^2\rangle) \tag{4}$$

In practice, the reflectivity is sensitive to interfacial thicknesses ranging from 5 to 200 Å. For non-Fickian diffusion the reflectance takes a different and, often, nonanalytical form.

Tables 2 and 3 give a compilation of the bilayers investigated in this study and of their differences following annealing. Since neutron reflectivity is nondestructive, successive annealing can be performed on the same specimen, minimizing systematic errors

Table 3

bilayer sample	top layer thickness (Å)	annealing time at 155 °C (min)	$\langle z^2\rangle^{1/2}$	$\langle z^4\rangle^{1/4}$
(1) D1.1M/H1.03M	850	15	137	190
(2) 10% D1.1M/H1.03M	1170	15	149	212
		32.5	192	265
		212.5	*a*	*a*
(3) H1.03M/10% D1.1M	610	5	105	152
(4) H1.03M/50% D1.1M	615	5	105	152
(5) 50% D1.1M/D1.1M	800	15	130	180
(6) D1.1M/H1.03M	850	15	138	196
		23.5	162	225
(7) H1.03M/D1.1M	1080	5	82	120
		15	122	174
		35	171	231

[a] Widths are too large to be measured accurately.

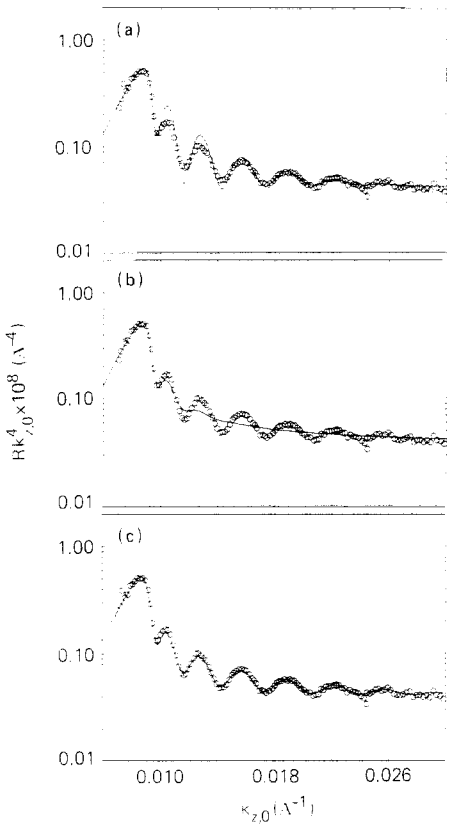

Figure 2. Rk^4 as a function of k for a bilayered sample of d-PS ($M \sim 1\,150\,000$) on top of h-PS ($M \sim 1\,000\,000$) after annealing for 15 min at 155 °C. The circles are experimental data while the solid lines in (a) and (b) correspond to conventional fits with widths of 80 and 175 Å, respectively. The solid line in (c) corresponds to a profile with a reptation width of 225 Å and an interface gap of 0.3 in d-PS volume fraction convoluted with a Rouse width of 50 Å.

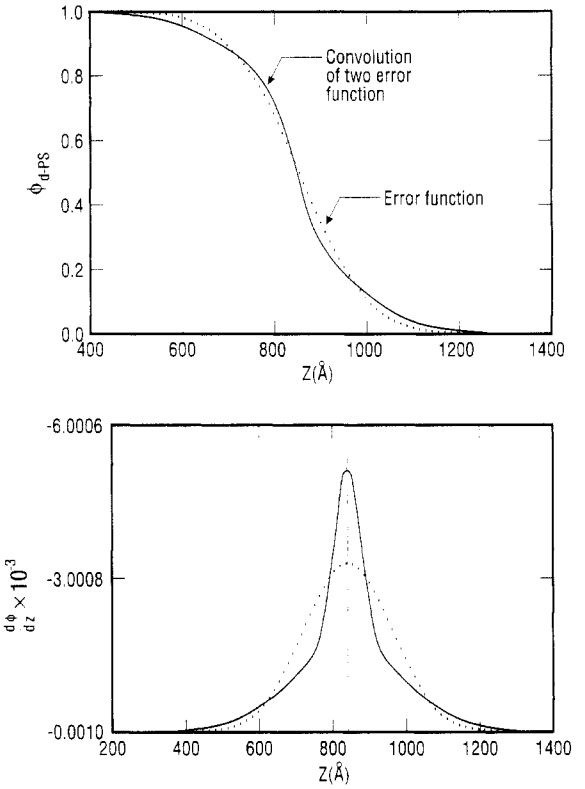

Figure 3. (a, Top) Real space profile for the bilayered sample whose reflectivity was shown in Figure 2 as fit by the Rouse convoluted reptation profile (solid line) and the conventional error function profile (dotted line). (b, Bottom) Derivative of the concentration profiles shown in a. The solid and dotted line correspond to the Rouse convoluted reptation profile and the conventional profile, respectively.

arising from different sample preparations. In some cases, the temperature in a series of experiments was increased or decreased to avoid impractically long or short annealing times. The normalization of these results to a common temperature will be discussed later. In the experiments it was noticed that even at time zero there was a finite interfacial width between the layers ranging from 7 to 18 Å. This interfacial width was quadratically subtracted at all subsequent times. The presence of this finite width initially is hardly surprising since even in the ideal case, where there are no imperfections due to sample preparation, an interfacial width corresponding to the separation distance between segments of the polymer (~5 Å) is expected.

Analysis of the Results

(A) The Moment Method. The ultimate goal of the reflectivity measurements is to determine the variation in the concentration profile of h-PS and d-PS segments across the interface as a function of time. However, there is no means, at present, to directly invert the reflectivity. Instead, model concentration profiles were used to calculate the reflectivity as a function of the neutron momentum, and this was compared with the experimental data. Over certain ranges of annealing times, eq 3 was found to be unsuitable for describing the variation in the scattering density across the interface. Instead a symmetric concentration profile defined by

$$\frac{dc}{dz}(z) = \sum_i a_i \exp(-[z^2/\langle z_i^2 \rangle]) \qquad (5)$$

was used. Here, the interface was assumed to be at the origin at all times.

In all cases, the sum of two Gaussian functions was sufficient to yield a suitable fit to the data. For instance, in Figure 2, the reflectivity of a d-PS(1M)/h-PS(1M) sample is shown as measured after an annealing time corresponding to one-half of the estimated reptation time. Panels a and b of Figure 2 show that using only a single error function with $\sigma = 80$ Å fits the data only for $k > 0.016$ Å^{-1} while with $\sigma = 175$ Å agreement with the data only for $k < 0.011$ Å^{-1} is found. This suggests that the concentration profile across the interface is described by two widths, one small and one large, to accommodate the observed reflectivity data. Figure 2c shows that excellent agreement with the reflectivity data can be achieved with such a profile. Here a concentration gradient with a width of 225 Å had a relative weight of 70%; the remaining 30% was a Gaussian function with a width of 50 Å. This concentration profile and its derivative are compared to the conventional error function profile in Figure 3a,b. The sensitivity of neutron reflection arises from the striking difference between the derivatives of the two profiles.

A compact way to present the experimental findings is to evaluate the moments of the concentration gradient, $\langle z^n \rangle$, defined as

$$\langle z^n \rangle = \frac{\int_{-\infty}^{\infty} z^n \left[\frac{d\phi(z)}{dz}\right] dz}{\int_{-\infty}^{\infty} \left[\frac{d\phi(z)}{dz}\right] dz} \qquad (6)$$

The first moment of the distribution around the interface ($z = 0$) remains zero, indicating that there is no net mass flow between the two layers. Only $\langle z^2 \rangle$ and $\langle z^4 \rangle$ were evaluated for the interdiffusion profiles. These are given

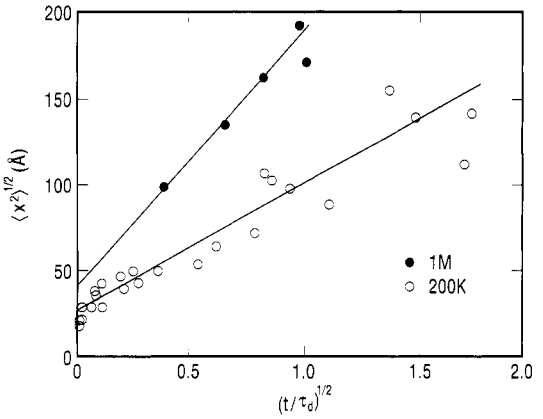

Figure 4. $\langle x^2\rangle^{1/2}$ as a function of $(t/\tau_d)^{1/2}$ for all samples. The straight lines are a guide to the eye and are discussed in the text.

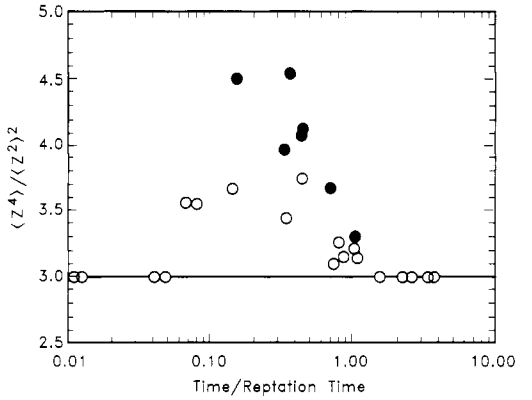

Figure 5. Normalized fourth moment of the concentration profiles as a function of reduced time normalized to the reptation time for PS with molecular weights of ~200 000 (○) and 10^6 (●).

in Tables 2 and 3 for all the specimens studied. Figure 4 shows the variation of $\langle x^2\rangle$ as a function of time, normalized to the reptation time. Figure 5 shows the time evaluation of $\langle z^4\rangle/\langle z^2\rangle^2$. For a conventional error function profile, this ratio assumes a value of 3. For ratios larger than 3, the concentration gradient has longer tails than a Gaussian as, for example, with the sum of two Gaussians. On the other hand, a ratio less than 3 is indicative of a sharper distribution, for instance, in the difference of two Gaussians. Consequently, deviations from a value of 3 will isolate time intervals over which nonconventional profiles are observed. The use of the moments will tend to reduce systematic errors between data sets.

(B) The WLF Relation. The data in Tables 2 and 3 have been reduced in time to temperatures of 120 and 155 °C. The time has been then normalized to the reptation time. This procedure places a large body of data on a time scale which spans many orders of magnitude, thereby allowing the observation of trends in the evolution of the concentration profiles. The data reduction was achieved via the use of the WLF time–temperature superposition principle. The relation is based on two assumptions: that the viscosity of the polymer obeys an Arrhenius law and that the free volume can be expanded in a power series of $(T - T_f)$, where T_f is the fictive temperature, i.e., the temperature where motions cease, and only the linear terms are retained. Here, relaxations measured at different temperatures in a time t occur at the reference temperature in a time $a_T t$ where a_T is the shift factor. For polystyrene with molecular weights in excess of 10^5 Tassin et al.[32] determined that a_T is given by

$$\log a_T = \frac{-9.066(T - 120)}{69.8 + (T - 120)} \tag{7}$$

where a reference temperature of 120 °C is used. This equation is valid provided that the measurement temperature T is within 50 °C of the reference temperature. Near or below T_f of the polymer eq 7 is not valid. PS has a T_f of ~50 °C.

As a limited test of the validity of eq 7, two identical specimens (samples 8 and 9 in Table 1) were annealed at 116 and 125 °C. Figure 6 shows $\langle z^2\rangle$ for the two sets of data where the data obtained at 125 °C (open squares) had been reduced (WLF shifted) to 116 °C by use of eq 7. There is a systematic overcorrection in time of the 125 °C data by ~20% due, possibly, to the fact that the temperature chosen were close to T_g. For all the other cases which are further removed from T_g, it can be argued that the errors will be less. For subsequent data presented in this article the reduced time scale will span more than 6 orders of magnitude.

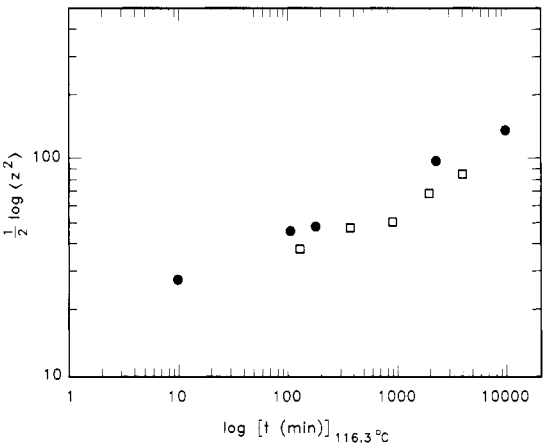

Figure 6. Root mean square displacement as a function of annealing time for samples 8 (hollow squares) and 9 (solid circles) of Table 1 annealed at 125 and 116.3 °C, respectively. The data of sample 8 have been shifted in time to an effective temperature of 116.3 °C using the time–temperature superpositioning principle given by eq 8.

(C) Thermodynamic Slowdown. Up to this point the interfacial profiles have been treated with the assumption that deuteration of the polymer chain does not affect the mixing process. The small repulsive interaction between deuterated and protonated monomers modifies the Flory–Huggins expression for the free energy of mixing for a binary mixture:

$$F/k_BT = N^{-1}[\phi \ln \phi + (1 - \phi) \ln(1 - \phi)] + \chi\phi(1 - \phi) \tag{8}$$

where χ is the segmental interaction parameter between polymers of equal degree of polymerization N. For polystyrene $\chi = 0.2/T - 2.9 \times 10^{-4}$. As shown by Bates and co-workers,[30,31] the small repulsive interaction between deuterated and protonated monomers can, for high molecular weight polymers, give rise to an upper critical solution temperature (UCST) above the glass transition temperature. For instance, for a molecular weight of 2.2×10^5 the UCST is below T_g whereas for a molecular weight of 1×10^6 the UCST is at 140 °C.

As a result, the mutual diffusion coefficient D_M is not constant but varies with the concentration ϕ according to the expression

$$D_M(\phi) = D^*[1 - 2N\phi(1 - \phi)\chi] \tag{9}$$

The minimum value of D_M is, for $M = 2 \times 10^5$, equal to $0.85D^*$, but for $M = 1 \times 10^6$, $D_M = 0.15D^*$. This has deep consequences not only on the slowing down of the diffusion

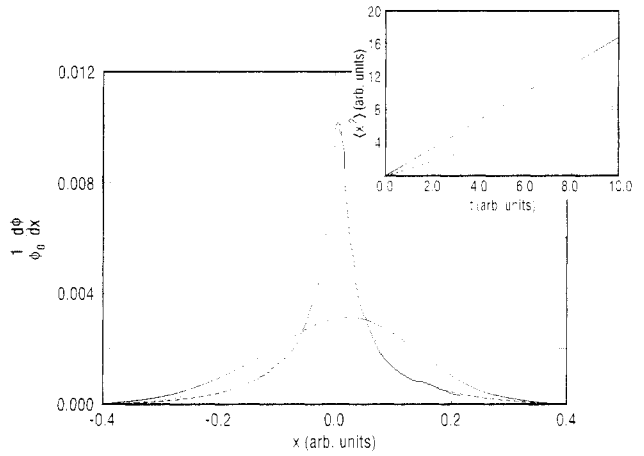

Figure 7. Calculated diffusion profile for a diffusion coefficient given by eq 9, $\chi N = 3.4$: dashed line, $\phi_\infty = 1$; dotted line, $\phi_\infty = 0.5$; solid line, $\phi_\infty = 0.1$. In the inset the variation of $\langle \alpha^2 \rangle$ with time is shown (the lines for $\phi_\infty = 0.5$ and $\phi_\infty = 1$ are indistinguishable).

but also on the functional shape of the concentration profile. Both the concentration and temperature dependences of this thermodynamic slowdown were exhaustively treated by Green and Doyle[33] in a series of interdiffusion measurements on h-PS/d-PS mixtures using forward recoil spectrometry.

The derivative of the concentration profile obtained by numerically solving eq 9 for the interdiffusion of two layers of polymers of molecular weight 1×10^6, one fully protonated and the second fully deuterated, is presented in Figure 7. The profile does not have the shape of a single Gaussian but instead is very similar to the one used to fit the reflectivity. In fact, the reflectivity calculated from this profile fits the experiment very well. To resolve the ambivalence of interpretation of the data, interdiffusion measurements were done on bilayer samples with 0 and 50% dPS and 0 and 10% dPS between the top and bottom layers. The relative calculated profiles are also shown in Figure 7. For the 50% sample, the calculated profile is skewed as a result of the asymmetric diffusion, and the position of maximum concentration gradient shifts from the original interface. This is the quantity that, in practice, defines the thickness d of a layer in reflectivity (eq 1). Yet experimentally, no shift of the thickness oscillations was observed for the 0–50% samples.

The gradient of the calculated concentration profile (cf. eq 9) for the 0–10% sample has a shape *much* closer to a Gaussian. At large dilutions, the thermodynamic slowdown becomes insignificant. This is corroborated by the variation of $\langle x^2 \rangle$ versus time, shown in the insert. For the 0–10% sample, the evolution of the second moment is only slightly slower than for $\chi = 0$, while it is much slower for the higher deuterium-enriched samples. In contrast, in the reflectivity experiments the diffusion proceeds at the same rate for all three kinds of samples (Table 3) with a negligible shift of the initial interface position.

Discussion

It is hardly surprising that $\langle x^2 \rangle$ grows linearly with time. Since the diffusion coefficient is solely dependent on concentration, the diffusion equation can be expressed solely in terms of a rate variable $y = xt^{-1/2}$. Basically, the diffusion profile retains the same shape in time, although this does not have the Gaussian form it assumes for constant diffusion coefficient. However, this is still conventional Fickian diffusion which describes the center-of-mass motion and not the reptative motions that cause $\langle x^2 \rangle$ to be smaller for $t < \tau_d$ (cf. Figure 1). Thus, the thermodynamic slowdown could be probed in reflectivity measurements only if the measurements could be carried out for times significantly beyond the reptation time.

The evolution of $\langle x^2 \rangle$ versus time is presented in Table 2 and, for visual purposes, in Figure 4. One must be cautious not to overinterpret the data. For instance, if we had chosen to present the data in a log–log manner, a power law exponent could be "determined". However, if anything modifies the variation in $\langle x^2 \rangle$ with time such that $\langle x^2 \rangle \propto t^\beta + a$, then, over a limited time range, any value of β could be determined depending on the range of t chosen. In Figure 4, it becomes apparent that a rapid relaxation takes place at short time (but not at $t = 0$, since the original broadening of the interface has been removed). The data are plotted as $\langle x^2 \rangle^{1/2}$ versus $t^{1/2}$, a choice that renders the reading of the ordinate very transparent.

While an initial rapid relaxation may be in line with a Rouse broadening, the sparsity of the experimental points does not allow a detailed comparison with the predicted evolution of the second moment as described in Figure 4. Roughly speaking, $\langle x^2 \rangle^{1/2} = at^{1/2} + b$. If this expression is rewritten as $\langle x^2 \rangle = a^2 t +$ other terms, a comparison can possibly be made with the marker diffusion coefficient given by $\langle x^2 \rangle = 2D^* t$. For both molecular weights we obtain diffusion coefficients from the slopes that are approximately 15% lower than bulk D^* values. This suggests that the average diffusion coefficient over times up to τ_d is less than bulk values, as might be expected for reptating molecules at short times.

The neutron reflection data provide, in each run, much more information than just the value of $\langle x^2 \rangle$. Shown in Figure 5 are the values of $\langle z^4 \rangle / \langle z^2 \rangle^2$ as a function of reduced time for h-PS/d-PS pairs with molecular weights of ~233 000 (open circles) and $\sim 10^6$ (filled circles). For the lower molecular weight pairs a clear trend in the data is observed. For times less than $\sim \tau_R$, $\langle z^4 \rangle / \langle z^2 \rangle^2 = 3$. As the time increases, the ratio is seen to deviate from the value of 3, reaching a maximum and then returning to the value of 3 for times greater than or equal to τ_d. The deviations of $\langle z^4 \rangle / \langle z^2 \rangle^2$ from 3.0 for times between τ_R and τ_d show that the interfacial profiles are sharper than expected for conventional diffusion arguments. The picture that emerges from the time dependence of $\langle z^4 \rangle / \langle z^2 \rangle^2$ is consistent with the prediction of the reptation theory. Initially segments of the polymer chain less than an entanglement length can freely move within a tube defined by local constraints, and they establish a conventional but diffusion-limited profile across the interface. At longer times the motion takes place by movement of the chain along its own contour: only the ends of the chains can diffuse across the interface. After one reptation time, the center of mass of the molecule moves with diffusive motion and the density profile regains the form of an error function.

The 10^6 molecular weight pair shows much larger deviations from the conventional ratio. The value of $\langle z^4 \rangle / \langle z^2 \rangle^2$ is larger for the higher molecular weight because the reptative motion occurs for a larger size molecule, while the segmental Rouse motion is independent of the molecule's size. However, the range of times studied is limited. Obtaining data for the 10^6 molecular pair at the short times is restricted by the requirement that the annealing temperature be substantially above the upper critical solution temperature, 140 °C.[30,31]

A more quantitative comparison of the real space profile with the reptation theory (or, for that matter, any alternative model) would entail a theoretical estimate of

$\langle x^4 \rangle$, $\langle x^2 \rangle$, and their evolution with time. It is auspicious that these quantities will soon become available. An even more direct and meaningful comparison with theory will be possible if this was cast to provide the density correlation function (and the reflectivity) along the lines shown by Binder[35] and Harden.[36]

Acknowledgment. The authors would like to thank E. J. Kramer, A. Mansour, S. Kumar, and M. Tirrell for their insightful comments and criticism during the course of this work. This work was supported in part (T.P.R.) by the U.S. Department of Energy, Office of Basic Energy Sciences, Grant No. DE-FG03-88ER45375. Work at Argonne was supported by the U.S. Department of Energy, BES-Materials Sciences, under Contract W-31-109-Eng-30.

References and Notes

(1) Kausch, H. H.; Tirrell, M. V. *Annu. Rev. Mater. Sci.* **1989**, *19*, 341.
(2) Klein, J.; Briscoe, B. J. *Proc. R. Soc. London* **1979**, *A365*, 53.
(3) Kramer, E. J.; Green, P. F.; Palmstrom, C. J. *Polymer* **1984**, *25*, 473.
(4) Green, P. F.; Palmstrom, C. J.; Mayer, J. W.; Kramer, E. J. *Macromolecules* **1985**, *18*, 501.
(5) Whitlow, S. J.; Wool, R. P. *Macromolecules* **1989**, *22*, 2648.
(6) de Gennes, P.-G. *J. Chem. Phys.* **1980**, *72*, 4756.
(7) de Gennes, P.-G. *Scaling Concepts in Polymer Physics*; Cornell University Press: Ithaca, NY, 1979.
(8) Edwards, S. F.; Doi, M. *The Theory of Polymer Dynamics*; Oxford University Press: Oxford, 1988.
(9) Graessley, W. W. *Adv. Polym. Sci.* **1974**, *1*, 16.
(10) Kremer, K.; Grest, G.; Carmesin, I. *Phys. Rev. Lett.* **1988**, *61*, 566.
(11) Richter, D.; Farago, B.; Fetters, L. J.; Huang, J. S.; Ewen, B.; Lartigue, C. *Phys. Rev. Lett.* **1990**, *64*, 12.
(12) Russell, T. P.; Karim, A.; Mansour, A.; Felcher, G. P. *Macromolecules* **1988**, *21*, 1890.
(13) Fernandez, M. L.; Higgins, J. S.; Penfold, J.; Wards, R. C.; Shakleton, C.; Walsh, D. J. *Polymer* **1988**, *29*, 1923.
(14) Karim, A.; Mansour, A.; Felcher, G. P.; Russell, T. P. *Phys. Rev. B* **1990**, *42*, 6846.
(15) Felcher, G. P.; Karim, A.; Russell, T. P. *J. Non-Cryst. Solids* **1991**, *131–133*, 703.
(16) Stamm, M.; Hüttenbach, S.; Reiter, G.; Springer, T. *Europhys. Lett.* **1991**, *14*, 451.
(17) Reiter, G.; Steiner, U. *J. Phys. II* **1991**, *1*, 659.
(18) Russell, T. P.; Deline, V. R.; Dozier, W. D.; Felcher, G. P.; Agrawal, G.; Wool, R. P.; Mays, J. W. *Nature* **1993**, *365*, 235.
(19) Rouse, P. E. *J. Chem. Phys.* **1953**, *21*, 1272.
(20) de Gennes, P.-G. *J. Chem. Phys.* **1971**, *55*, 572.
(21) de Gennes, P.-G. *C. R. Seances Acad. Sci.* **1989**, *308II*, 13.
(22) Tirrell, M. V.; Adolf, D.; Prager, S. *Lect. Notes Appl. Math.* **1984**, *37*, 1063.
(23) Prager, S.; Tirrell, M. V. *J. Chem. Phys.* **1981**, *75*, 5194.
(24) Kim, Y. H.; Wool, R. P. *Macromolecules* **1983**, *16*, 1115.
(25) Wool, R. P. *J. Elastomers Plast.* **1985**, *17*, 106.
(26) Zhang, H.; Wool, R. P. *Macromolecules* **1989**, *23*, 3018.
(27) Karim, A.; Arendt, B. H.; Felcher, G. P.; Arendt, B.; Russell, T. P. *Thin Solid Films* **1991**, *202*, 345.
(28) Karim, A.; Arendt, B. H.; Goyette, R. J.; Huang, Y. Y.; Kleb, R.; Felcher, G. P.; *Physica B* **1991**, *173*, 17.
(29) Karim, A. Ph.D. Thesis, Northwestern University, 1990.
(30) Bates, F. S.; Wignall, G. D.; Kohler, W. C. *Phys. Rev. Lett.* **1986**, *57*, 12.
(31) Bates, F. S.; Fetters, L. J.; Wignall, G. D. *Macromolecules* **1988**, *21*, 1086.
(32) Tassin, J. F.; Monnerie, L.; Fetters, L. J. *Macromolecules* **1988**, *21*, 2407.
(33) Green, P. F.; Doyle, B. L. *Phys. Rev. Lett.* **1986**, *57*, 2407.
(34) Binder, K. *J. Chem. Phys.* **1983**, *79*, 6387.
(35) Harden, J. *J. Phys. Fr.* **1990**, *51*, 1777.